Supporting Information

Diverse structures and dimensionalities in Zn(II), Cd(II) and Hg(II) metal complexes with Piperonylic acid

Daniel Ejarque [a], Francisco Sánchez-Férez [a], José A. Ayllón[a], Teresa Calvet[b], Mercè Font-Bardia [c], Josefina Pons [a,]*

[a]Departament de Química, Universitat Autònoma de Barcelona, 08193-Bellaterra, Barcelona, Spain

[b]Cristal·lografia, Mineralogia I Dipòsits Minerals, Universitat de Barcelona, Martí i Franquès s/n, 08028 Barcelona, Spain

[c]Unitat de Difracció de Raig-X, Centres Científics i Tecnològics de la Universitat de Barcelona (CCiYUB), Universitat de Barcelona, Solé i Sabarís, 1-3, 08028 Barcelona, Spain

Crystallographic data

For **1c**, the integration of the data using a orthorombic unit cell yielded a total of 31371 reflections to a maxim θ angle of 30.58º (0.70 Å resolution), of which 9625 were independent (average redundancy 3.259, completeness = 99.0%), R_{int} = 4.75%, R_{sig} = 5.89%) and 8246 (85.67%) were greater than $2\sigma(F^2)$. The calculated minimum and maximum transmission coefficients (based on crystal size) are 0.5731 and 0.7461. For **2**, the integration of the data using a monoclinic unit cell yielded a total of 23326 reflections to a maxim θ angle of 26.44º (0.80 Å resolution), of which 3061 were independent (average redundancy 7.620, completeness = 99.3%), R_{int} = 4.78%, R_{sig} = 3.07%) and 2942 (96.11%) were greater than $2\sigma(F^2)$. The calculated minimum and maximum transmission coefficients (based on crystal size) are 0.6276 and 0.7454. For **3**, the integration of the data using a monoclinic unit cell yielded a total of 75108 reflections to a maxim θ angle of 30.55º (0.70 Å resolution), of which 7516 were independent (average redundancy 9993, completeness = 99.9%), R_{int} = 6.40%, R_{sig} = 3.57%) and 5827 (77.53%) were greater than $2\sigma(F^2)$. The calculated minimum and maximum transmission coefficients (based on crystal size) are 0.6545 and 0.7461. For **4**, the integration of the data using a monoclinic unit cell yielded a total of 53325 reflections to a maxim θ angle of 30.59º (0.70 Å resolution), of which 4363 were independent (average redundancy 12.222, completeness = 99.7%), R_{int}= 8.45%, R_{sig} = 4.05%) and 3549 (81.34%) were greater than $2\sigma(F^2)$. The calculated minimum and maximum transmission coefficients (based on crystal size) are 0.3818 and 0.7461.

For **1c**, the final anisotropic full-matrix least-squares refinement on F^2 with 500 variables converged at R_1 = 6.11%, for the observed data and wR_2 = 17.03% for all data. For **2**, the final anisotropic full-matrix least-squares refinement on F^2 with 230 variables converged at R_1 = 7.76%, for the observed data and wR_2 = 18.00% for all data. For **3**, the final anisotropic full-matrix least-squares refinement on F^2 with 341 variables converged at R_1 = 5.43%, for the observed data and wR_2 = 14.82% for all data. For **4**, the final anisotropic full-matrix least-squares refinement on F^2 with 226 variables converged at R_1 = 2.96%, for the observed data and wR_2 = 5.48% for all data.

HR-ESI-MS

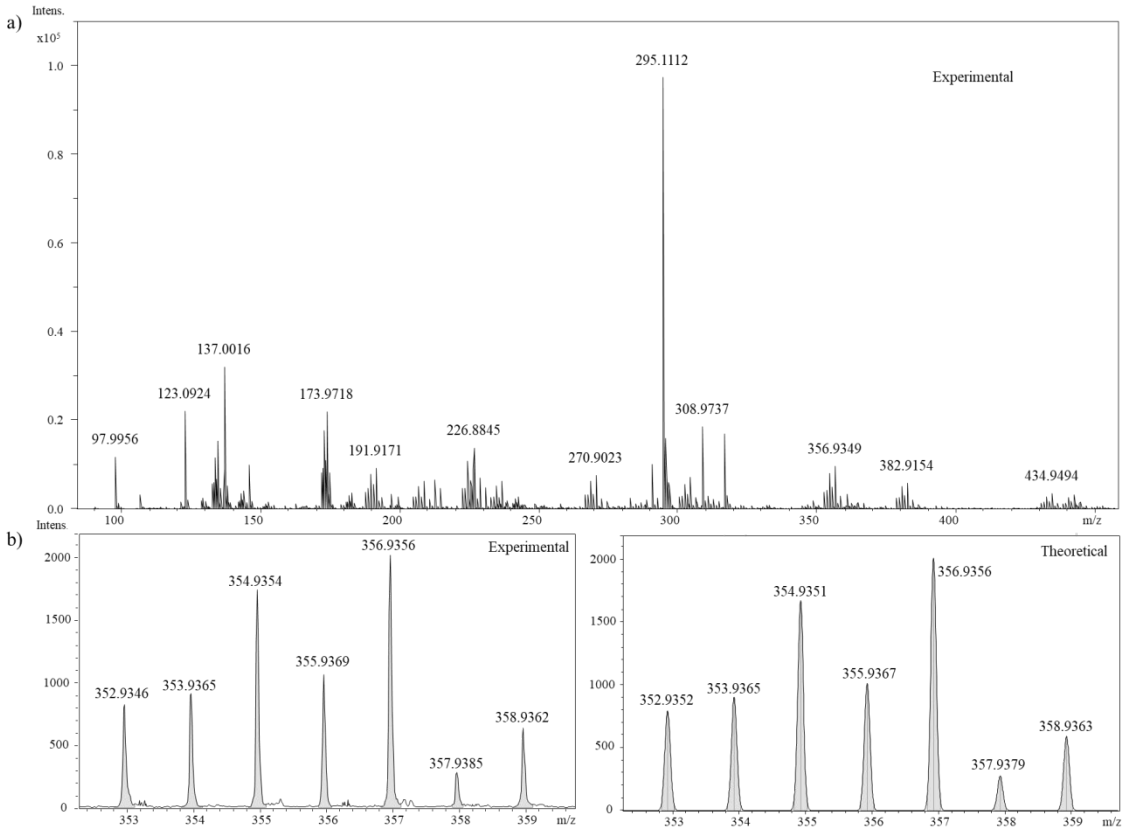

Figure S1. a. HR-ESI-MS spectra of **3**. b. In detail view of $[Cd(Pip)(DMSO)]^+$ fragment

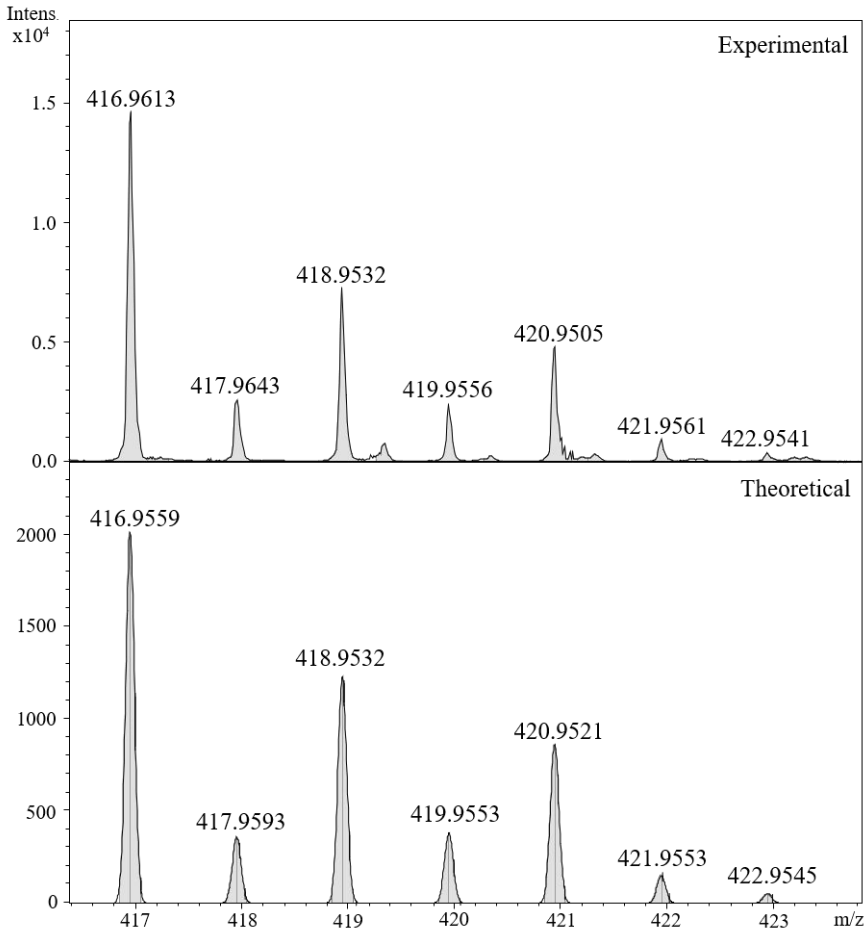

Figure S2. In detail view of [**1c** – $2H_2O$ + Na]$^+$ fragment in **1c**

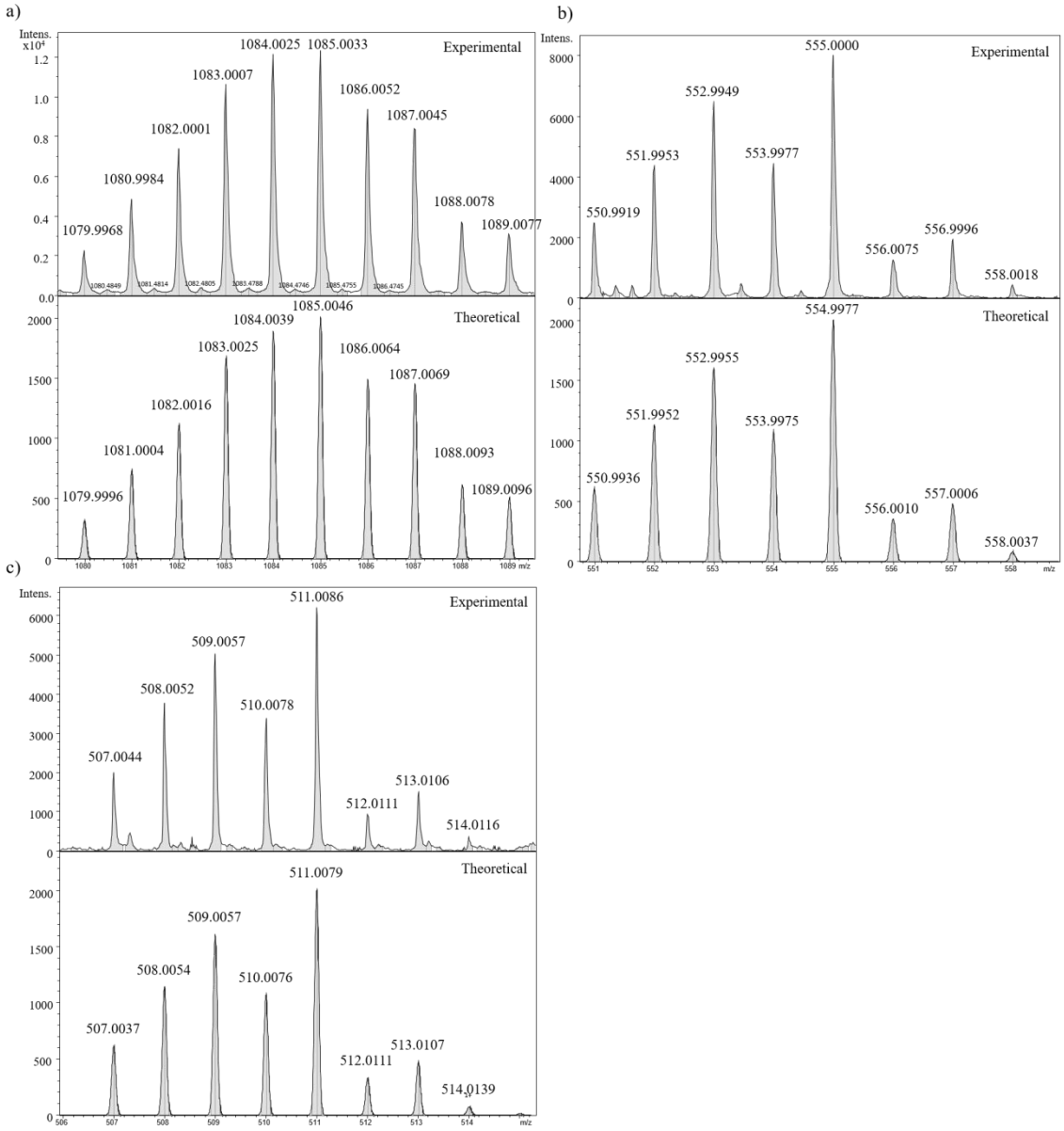

Figure S3. HR-ESI-MS spectra of compound **4**. In detail view of a. $[Hg_2(Pip)_4 + Na]^+$, b. $[Hg(Pip)_2 + Na]^+$ and c. $[\mathbf{4} - CO_2 + Na]^+$ fragments of **4**

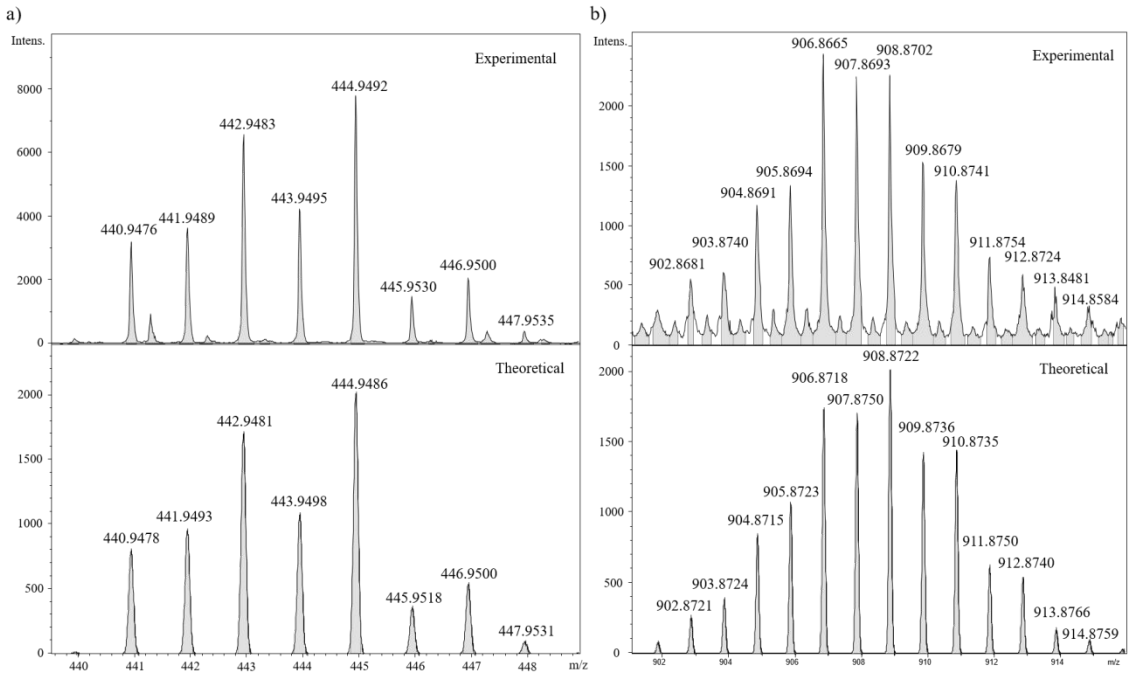

Figure S4. HR-ESI-MS spectra of compound **2**. In detail view of a. $[Cd(Pip)_2 + H]^+$ and b. $[Cd_2(Pip)_4 + Na]^+$ fragments

FTIR-ATR, ^{1}H and ^{13}C NMR spectroscopies

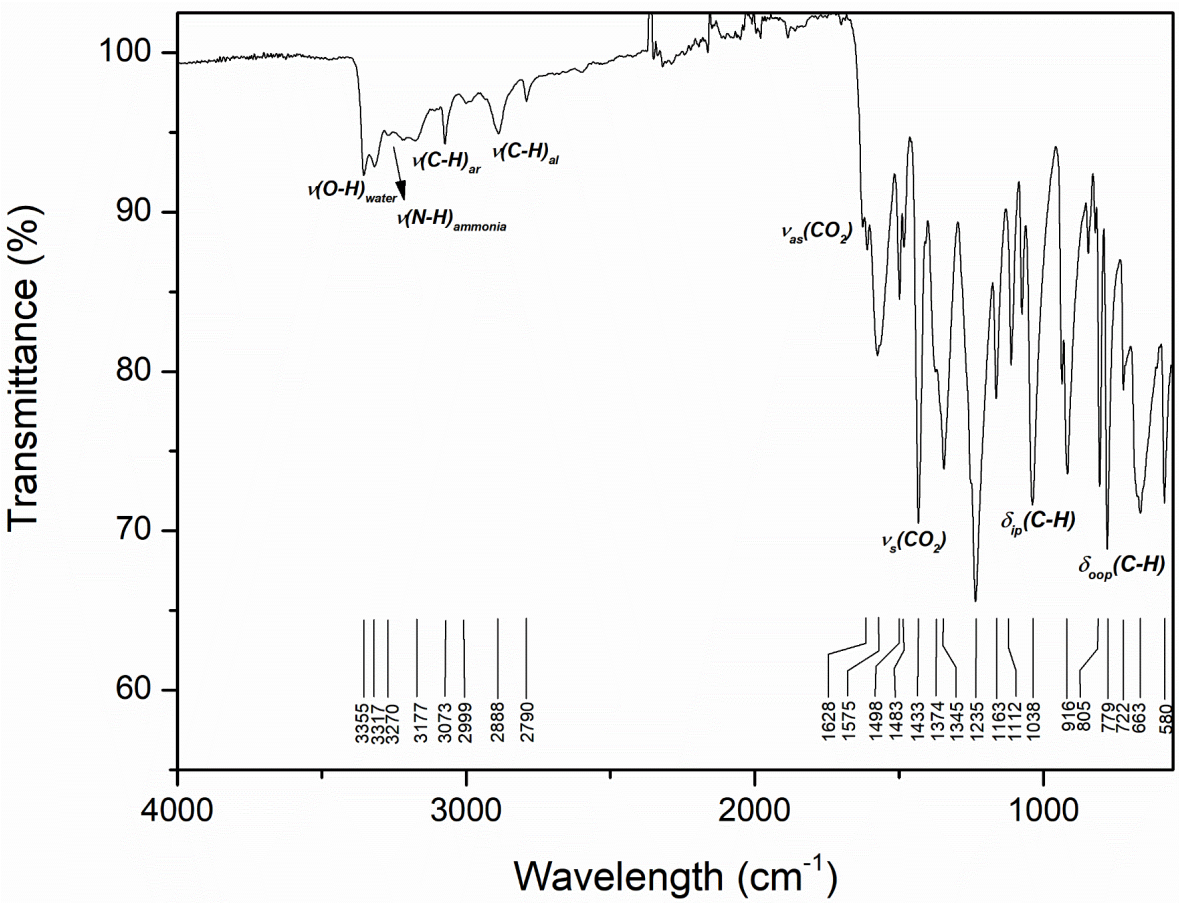

Figure S5. FTIR-ATR spectrum of compound $[Zn(Pip)_2(H_2O)(NH_3)]$ (**1b**)

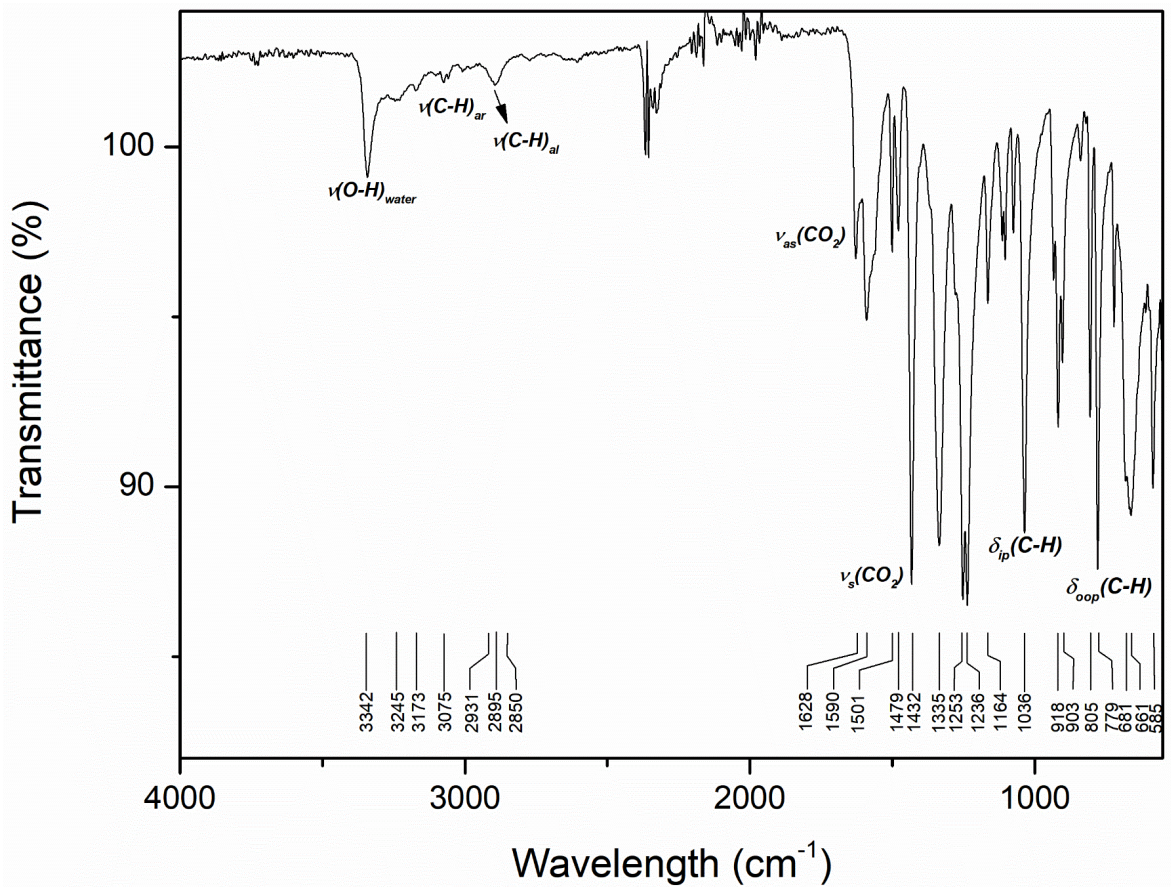

Figure S6. FTIR-ATR spectrum of compound $[Zn(Pip)_2(H_2O)_2]$ (**1c**)

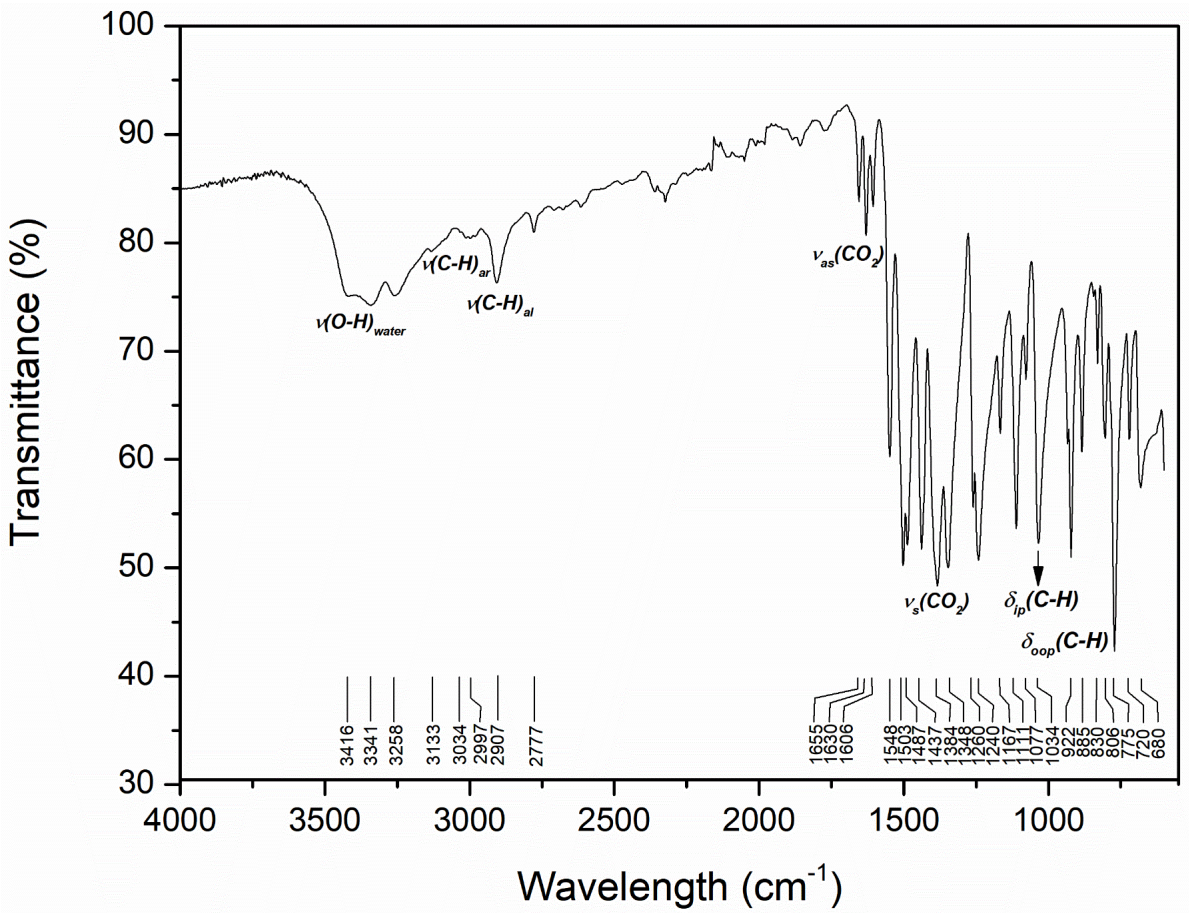

Figure S7. FTIR-ATR spectrum of compound $[Cd(\mu\text{-}Pip)_2(H_2O)]_n$ (**2**)

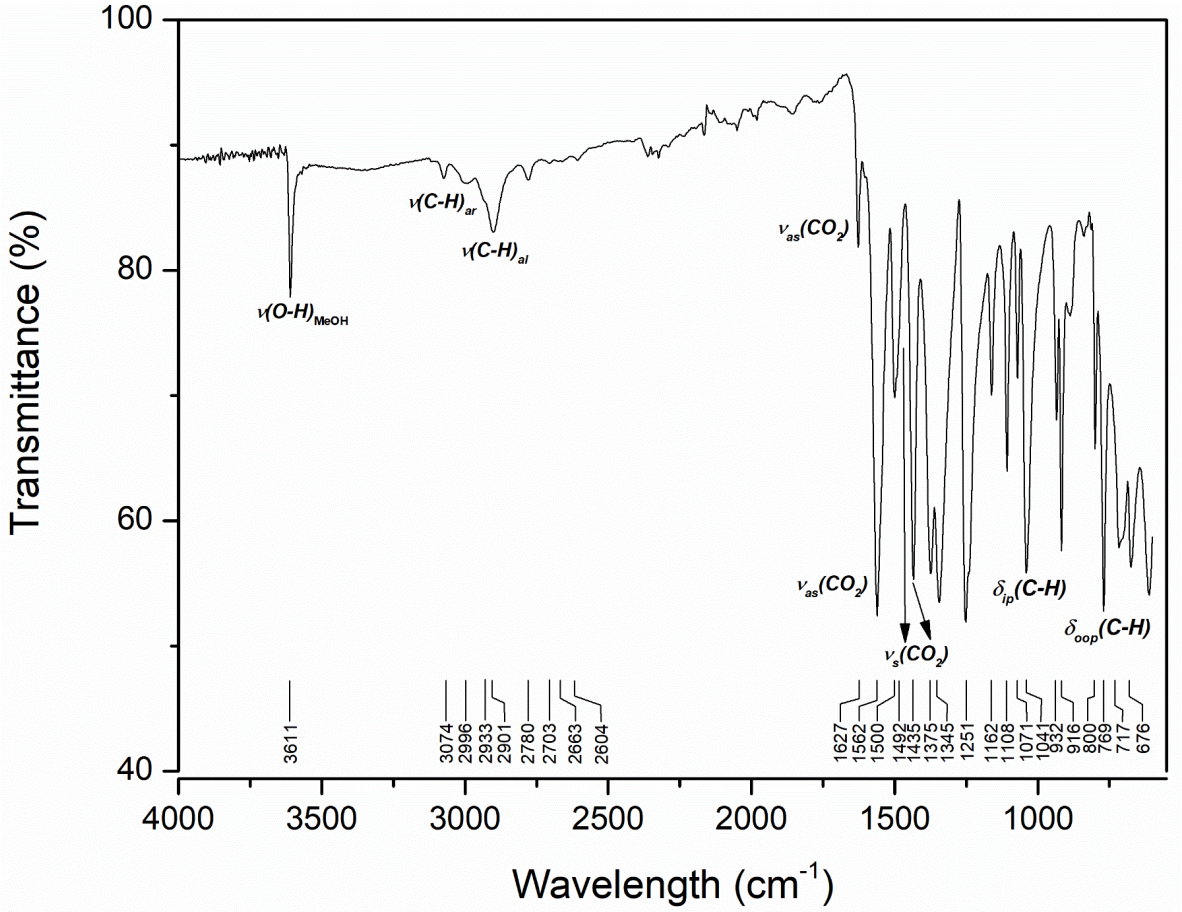

Figure S8. FTIR-ATR spectrum of compound $[Cd_3(\mu\text{-Pip})_6(MeOH)_2]_n$ (**3**)

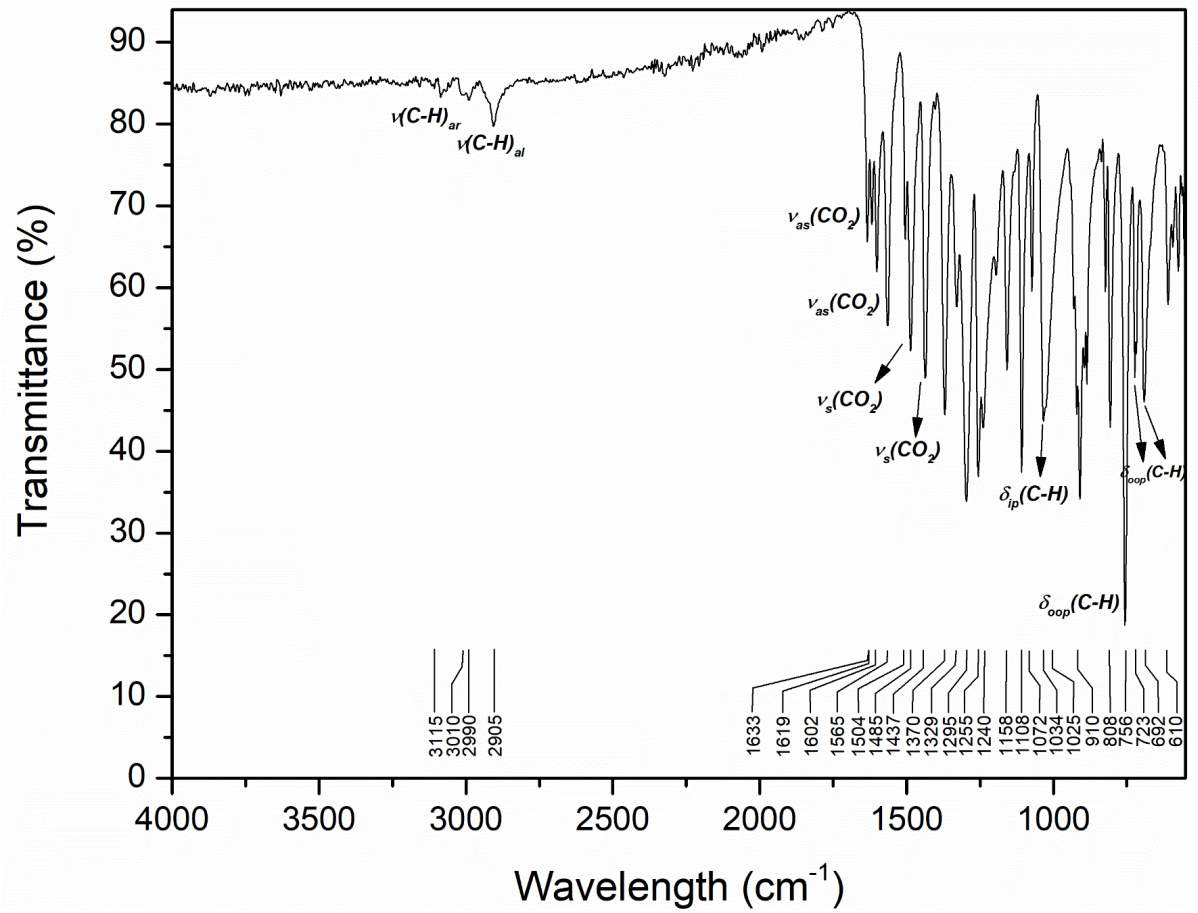

Figure S9. FTIR-ATR spectrum of compound $[Hg(\mu\text{-}Pip)_2]_n$ (**4**)

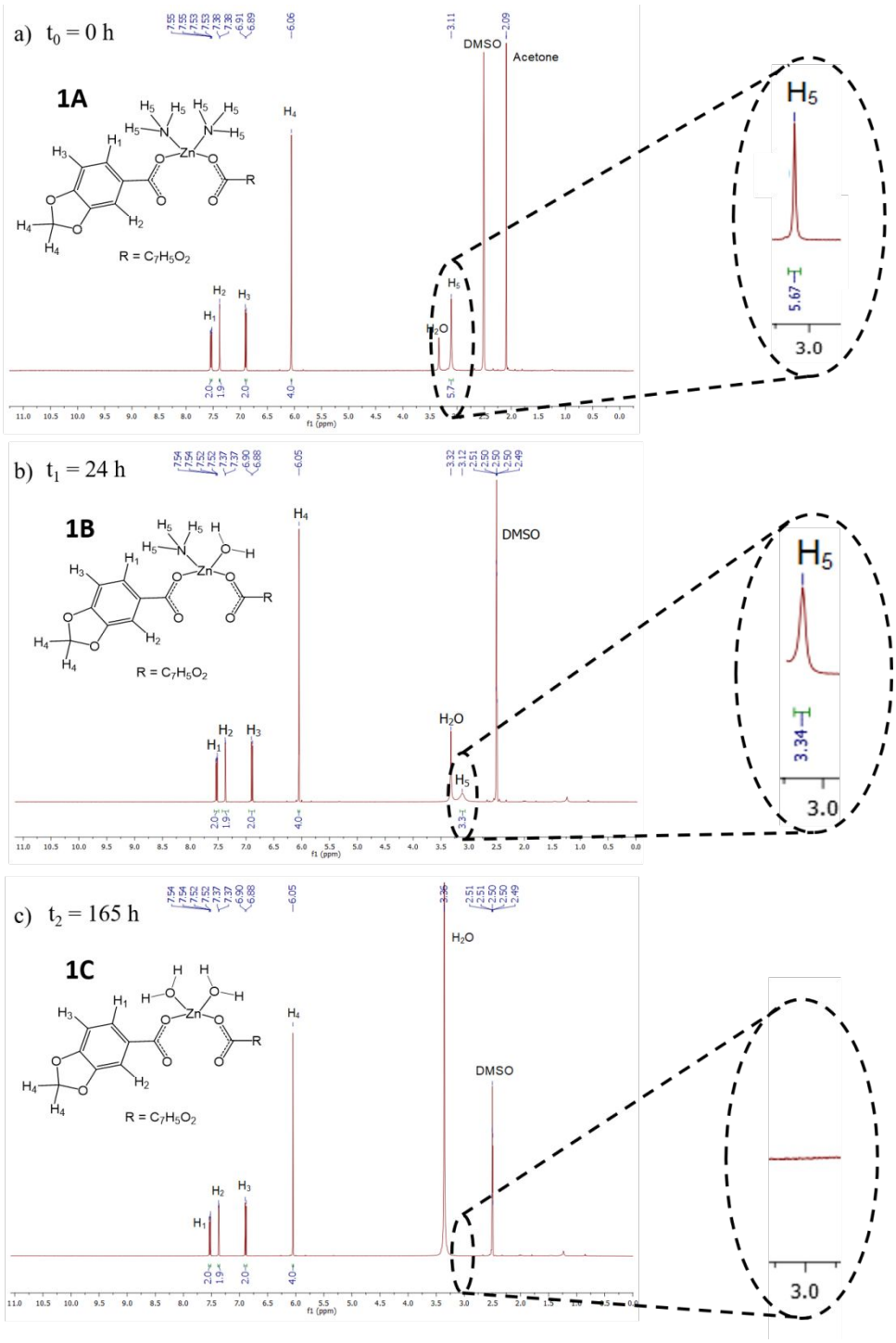

Figure S10. Time resolved ^{1}H NMR spectra in DMSO-d_6 solution of the same sample. Experiment a. at (t_0) (**1a**). b. after 24h (t_1) (**1b**) and c. after 7 days (t_2) (**1c**). In detail views of the peak around 3.1 ppm which is attributed to the ammonia molecules.

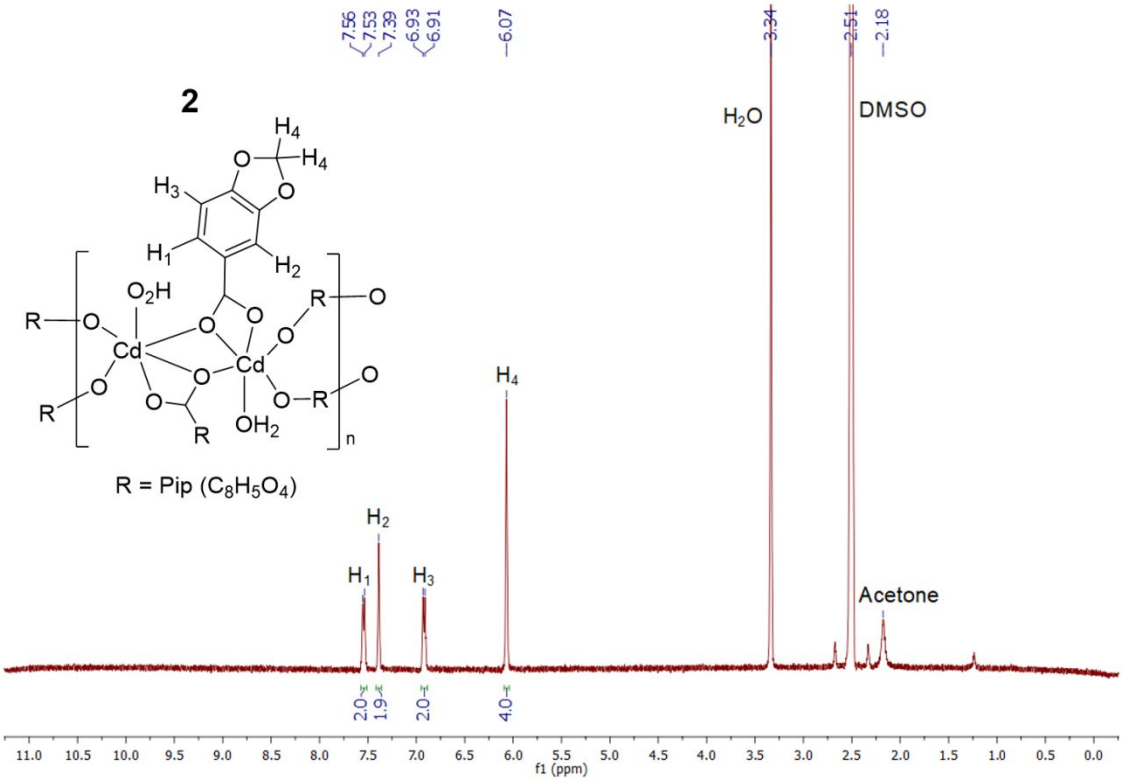

Figure S1. ^{1}H NMR spectrum of compound $[Cd(\mu\text{-}Pip)_2(H_2O)_2]_n$ (**2**)

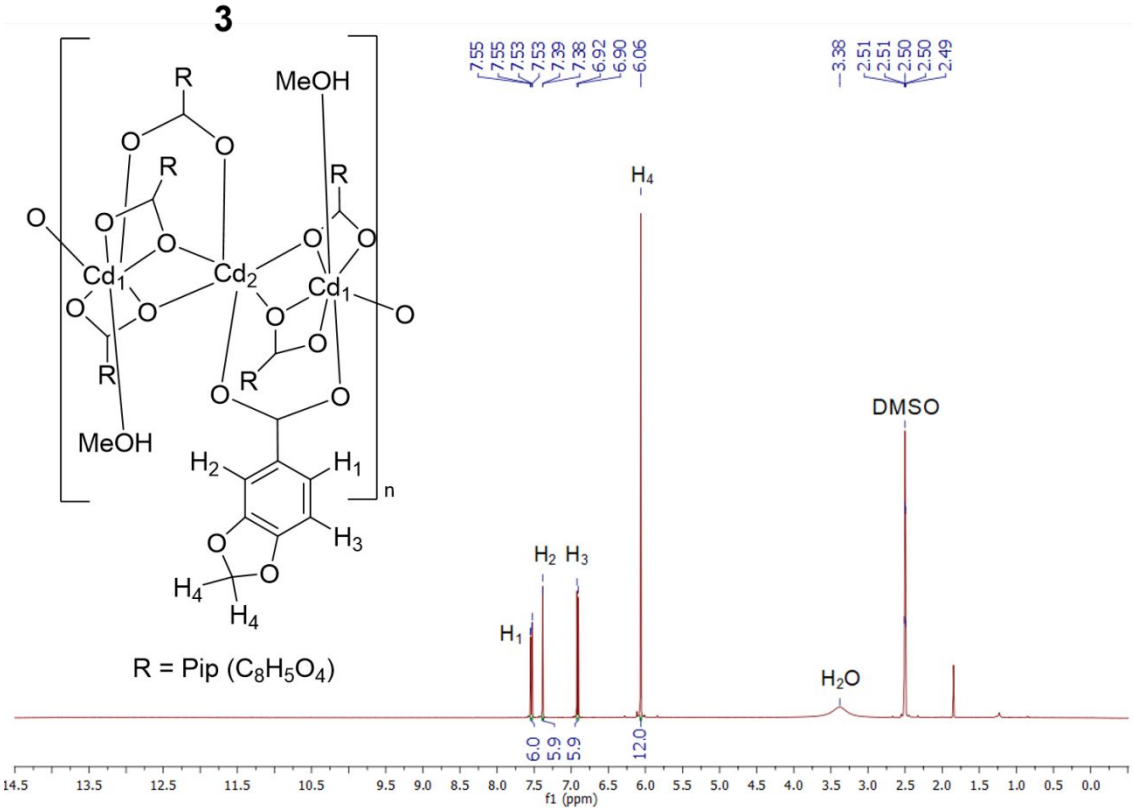

Figure S12. ^{1}H NMR spectrum of compound $[Cd_3(\mu\text{-}Pip)_6(MeOH)_2]_n$ (**3**)

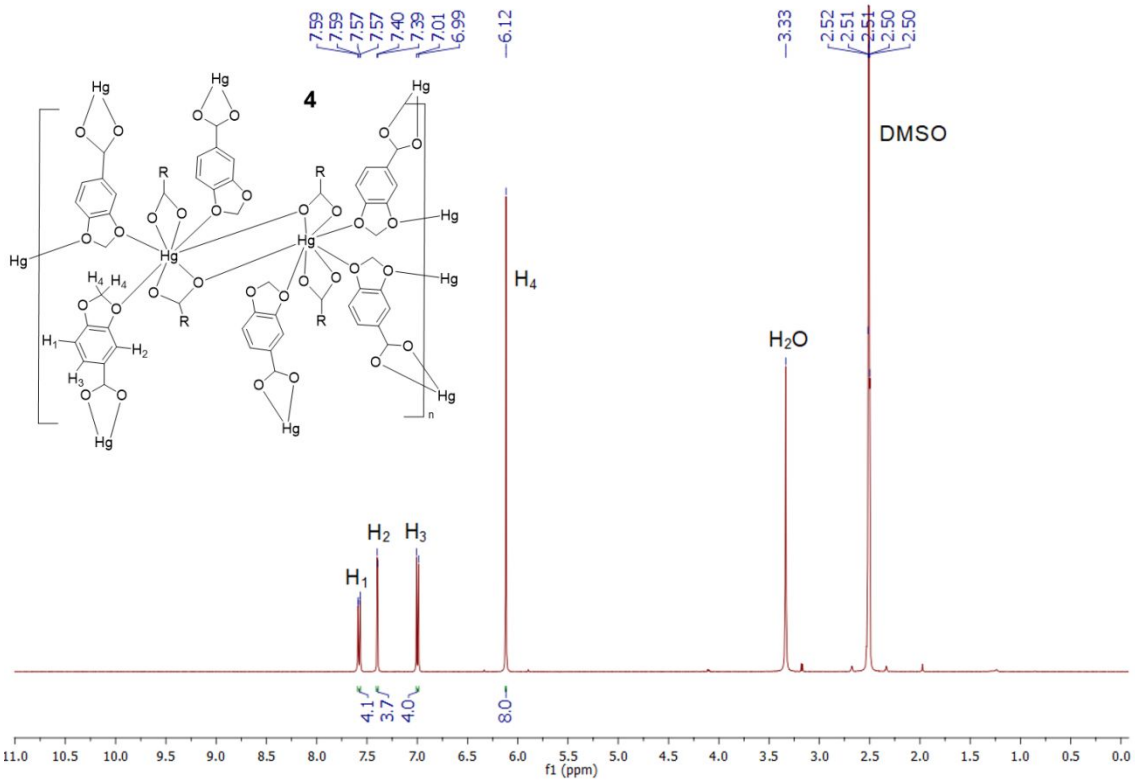

Figure S2. ^{1}H NMR spectrum of compound $[Hg(\mu\text{-}Pip)_2]_n$ (**4**)

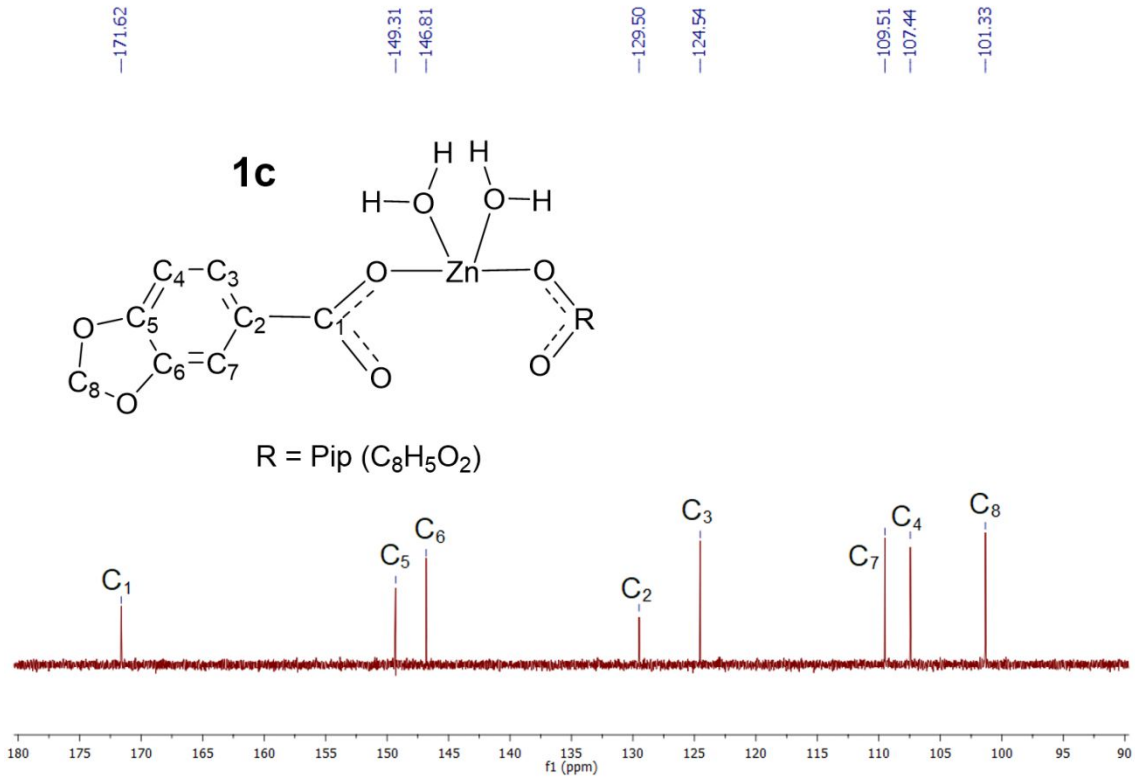

Figure S3. ^{13}C{^{1}H} NMR spectrum of compound $[Zn(Pip)_2(H_2O)_2]$ (**1c**)

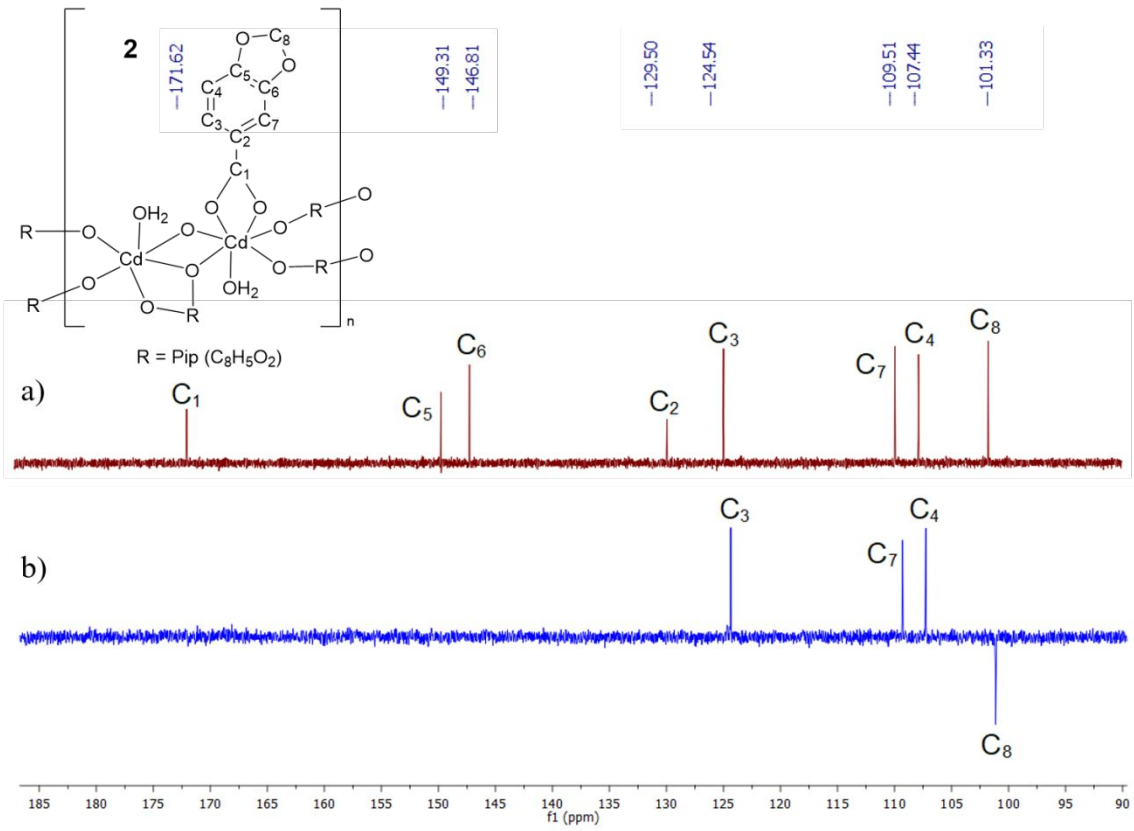

Figure S4. a. $^{13}C\{^{1}H\}$ NMR spectrum of compound $[Cd(\mu\text{-}Pip)_2(H_2O)_2]_n$ (**2**) b. DEPT-135 spectrum of compound $[Cd(\mu\text{-}Pip)_2(H_2O)_2]_n$ (**2**)

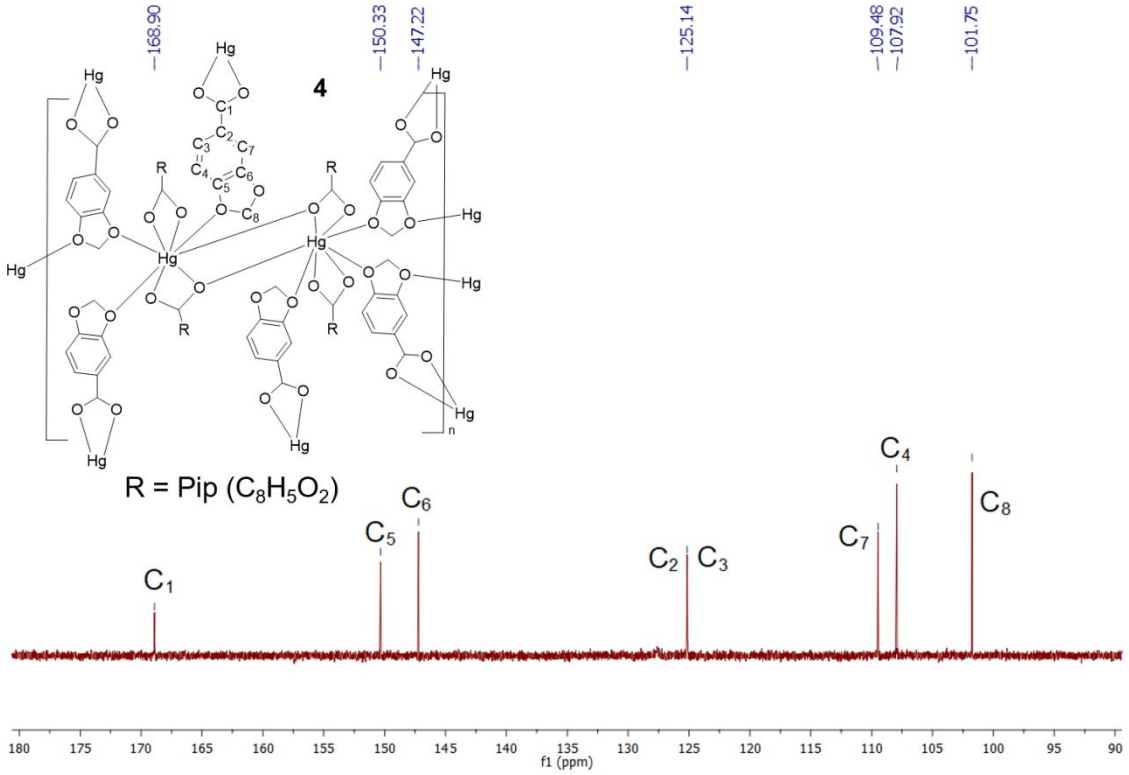

Figure S5. $^{13}C\{^{1}H\}$ NMR spectrum of compound $[Hg(\mu\text{-}Pip)_2]_n$ (**4**)

TG/DTA determinations

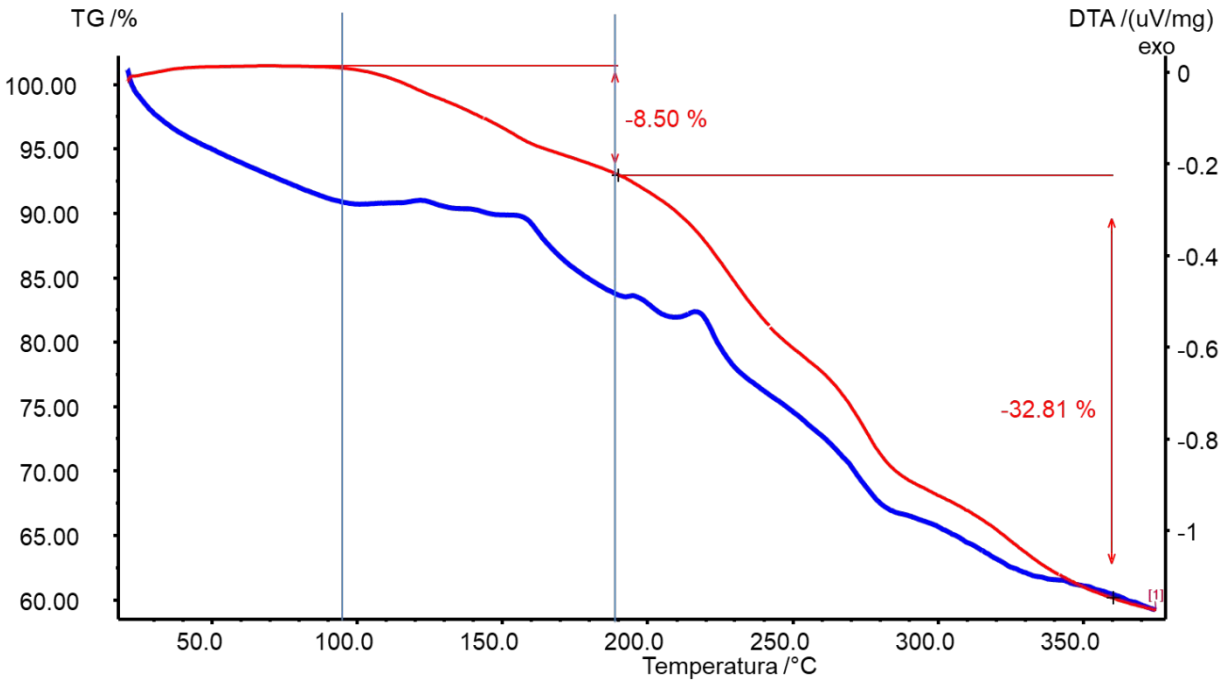

Figure S17. TG/DTA of compound **1c**

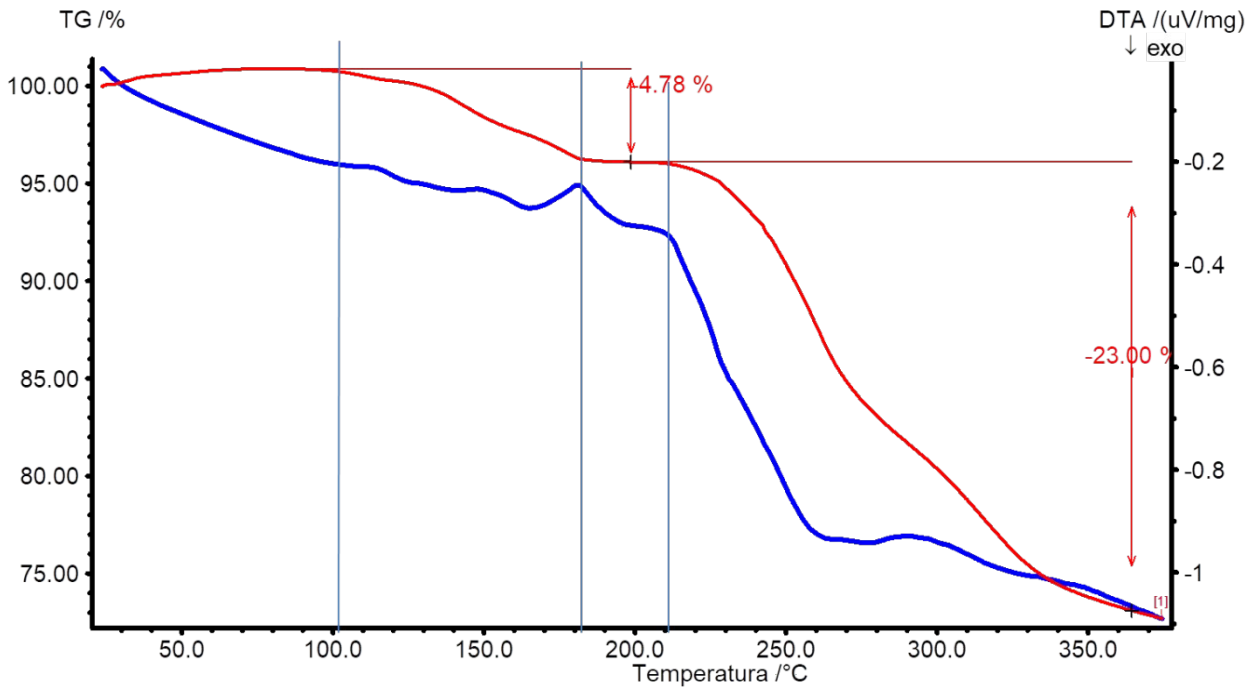

Figure S18. TG/DTA of compound **2**

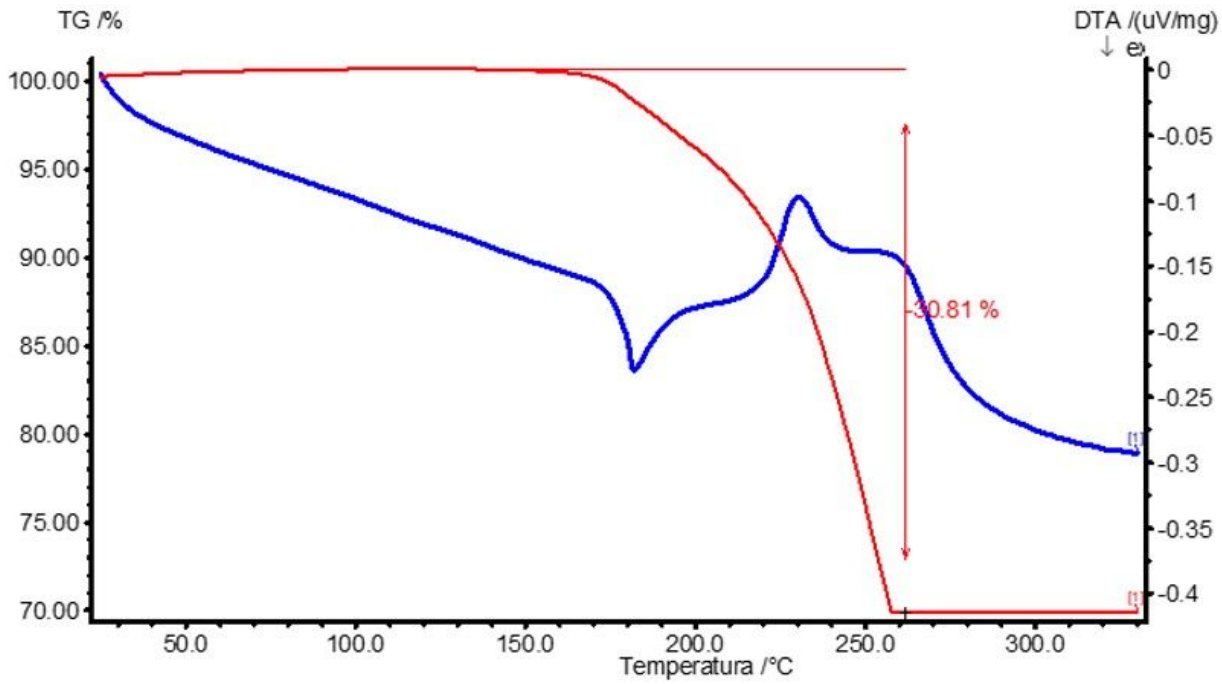

Figure S19. TG/DTA of compound **4**

UV-Vis spectroscopy

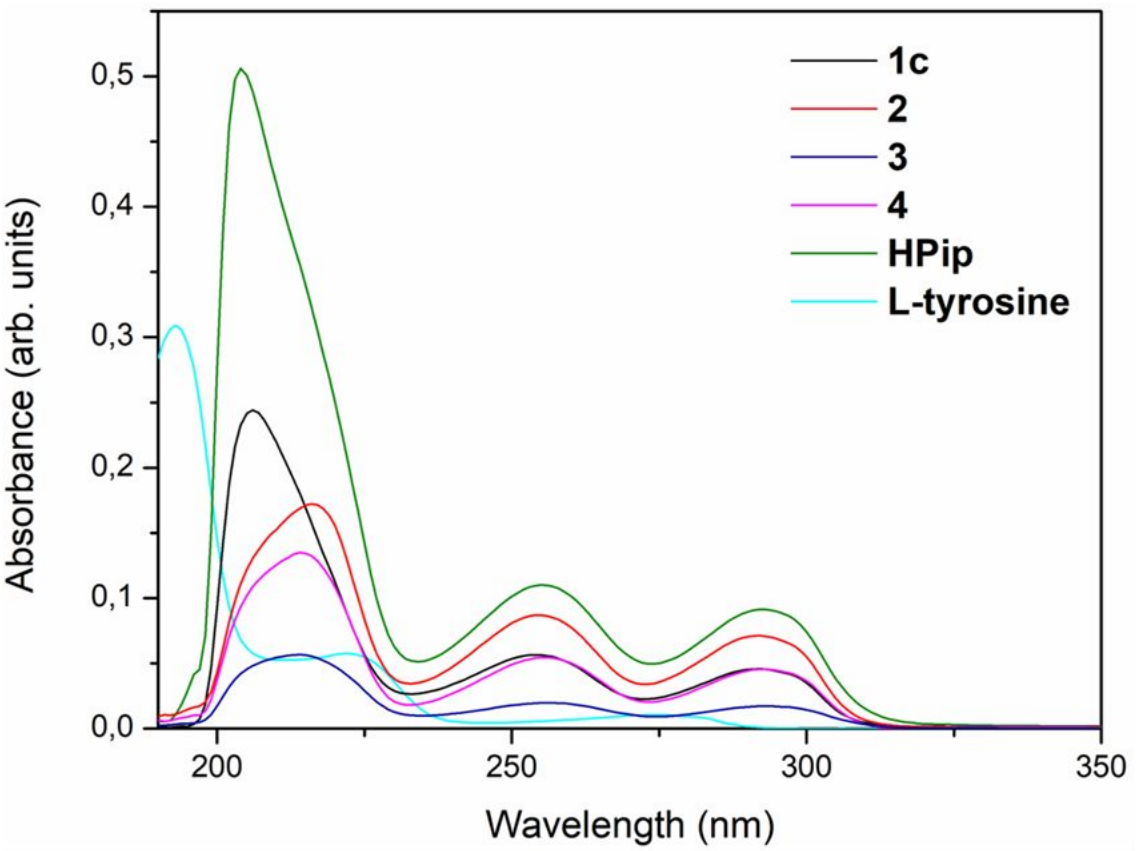

Figure S20. UV-Vis spectra of complexes **1c** (black line), **2** (red line), **3** (dark blue line) and **4** (pink line), HPip ligand (green line) and L-tyrosine (light blue line) in MeOH solution ($9.95 \cdot 10^{-7}$ M for the HPip and ~$1.00 \cdot 10^{-7}$ M for **1c**-**4** complexes) and Milli-Q water solution ($1.01 \cdot 10^{-4}$ M for L-tyrosine) at r.t.

Table S1. Detailed parameters extracted from the photoluminescence properties of HPip ligand and compounds **1c**-**4**.

	Abs (λ_{max}) (nm)	Emission (λ_{em}) (nm)	Quantum yield (φ_S)
HPip	204, 255, 292	352	0.0086
1c	206, 254, 292	369	0.019
2	216, 255, 292	369	0.033
3	214, 255, 292	353	0.053
4	214. 256. 293	363	0.12